Microparticle movements in optical funnels and pods

José A. Rodrigo,[1,*] Antonio M. Caravaca-Aguirre,[2] Tatiana Alieva,[2] Gabriel Cristóbal,[1] and María L. Calvo[2]

[1] *Instituto de Óptica, CSIC, Serrano 121, 28006 Madrid, Spain*
[2] *Universidad Complutense de Madrid, Facultad de Ciencias Físicas, Ciudad Universitaria s/n, 28040 Madrid, Spain*

**jose.a.rodrigo@optica.csic.es*

Abstract: Three-dimensional microparticle movements induced by laser beams with a funnel- and tubular pod-like structure, in the neighbourhood of the focal plane of an optical trapping setup, are experimentally studied. The funnel and pod beams constructed as coherent superpositions of helical Laguerre-Gaussian modes are synthesized by a computer generated hologram using a phase-only spatial light modulator. Particle tracking is achieved by in-line holography method which allows an accurate position measurement. It is experimentally demonstrated that the trapped particle follows different trajectories depending on the orbital angular momentum density of the beam. In particular applying the proposed pod beam the particle rotates in opposite directions during its movement in the optical trap. Possible applications of these single-beam traps for volumetric optical particle manipulation are discussed.

OCIS codes: (140.3300) Laser beam shaping; (140.7010) Trapping; (090.1760) Computer holography; (090.1995) Digital holography.

References

1. A. Ashkin, *Optical Trapping and Manipulation of Neutral Particles Using Lasers: A Reprint Volume With Commentaries* (World Scientific Publishing Company, 2006).
2. M. Padgett and L. Allen, "Light with a twist in its tail," Contemp. Phys. **41**, 275–285 (2000).
3. K. Ladavac and D. Grier, "Microoptomechanical pumps assembled and driven by holographic optical vortex arrays," Opt. Express **12**, 1144–1149 (2004).
4. A. Jesacher, S. Fürhapter, C. Maurer, S. Bernet, and M. Ritsch-Marte, "Holographic optical tweezers for object manipulations at an air-liquid surface," Opt. Express **14**, 6342–6352 (2006).
5. L. Paterson, M. P. MacDonald, J. Arlt, W. Sibbett, P. E. Bryant, and K. Dholakia, "Controlled rotation of optically trapped microscopic particles," Science **292**, 912–914 (2001).
6. E. G. Abramochkin and V. G. Volostnikov, "Spiral light beams," Phys. Usp. **47**, 1177 (2004).
7. T. Alieva, E. Abramochkin, A. Asenjo-Garcia, and E. Razueva, "Rotating beams in isotropic optical system," Opt. Express **18**, 3568–3573 (2010).
8. E. Abramochkin, S. Kotova, A. Korobtsov, N. Losevsky, A. Mayorova, M. Rakhmatulin, and V. Volostnikov, "Microobject manipulations using laser beams with nonzero orbital angular momentum," Laser Phys. **16**, 842–848 (2006).
9. A. Jesacher, S. Fürhapter, S. Bernet, and M. Ritsch-Marte, "Size selective trapping with optical cogwheel tweezers," Opt. Express **12**, 4129–4135 (2004).
10. K. Dholakia, M. P. MacDonald, P. Zemanek, and T. Cizmár, *Laser manipulation of cells and tissues methods in cell biology* (Elsevier, 2007), chap. Cellular and colloidal separation using optical forces, pp. 467–495.
11. D. G. Grier and Y. Roichman, "Holographic optical trapping," Appl. Opt. **45**, 880–887 (2006).
12. M. J. Padgett, J. E. Molloy, and D. Mcgloin, eds., *Optical Tweezers: Methods and Applications* (CRC Press, 2010).

#139978 - $15.00 USD Received 21 Dec 2010; revised 10 Feb 2011; accepted 13 Feb 2011; published 4 Mar 2011

13. A. E. Siegman, *Lasers* (University Science Books, 1986).
14. R. Zambrini and S. M. Barnett, "Angular momentum of multimode and polarization patterns," Opt. Express **15**, 15214–15227 (2007).
15. A. M. Caravaca-Aguirre and T. Alieva, "Orbital angular moment density of beam given as a superposition of Hermite-Laguerre-Gauss functions," in "PIERS 2011, Marrakesh," (2011).
16. R. Ozeri, L. Khaykovich, N. Friedman, and N. Davidson, "Large-volume single-beam dark optical trap for atoms using binary phase elements," J. Opt. Soc. Am. B **17**, 1113–1116 (2000).
17. J. Arlt and M. J. Padgett, "Generation of a beam with a dark focus surrounded by regions of higher intensity: the optical bottle beam," Opt. Lett. **25**, 191–193 (2000).
18. N. Bokor and N. Davidson, "A three dimensional dark focal spot uniformly surrounded by light," Opt. Commun. **279**, 229–234 (2007).
19. B. Sun, Y. Roichman, and D. G. Grier, "Theory of holographic optical trapping," Opt. Express **16**, 15765–15776 (2008).
20. E. Martín-Badosa, M. Montes-Usategui, A. Carnicer, J. Andilla, E. Pleguezuelos, and I. Juvells, "Design strategies for optimizing holographic optical tweezers set-ups," J. Opt. A, Pure Appl. Opt. **9**, S267 (2007).
21. F. C. Cheong, B. J. Krishnatreya, and D. G. Grier, "Strategies for three-dimensional particle tracking with holographic video microscopy," Opt. Express **18**, 13563–13573 (2010).
22. J. P. Kirk and A. L. Jones, "Phase-Only Complex-Valued Spatial Filter," J. Opt. Soc. Am. **61**, 1023–1028 (1971).
23. J. A. Davis, D. M. Cottrell, J. Campos, M. J. Yzuel, and I. Moreno, "Encoding amplitude information onto phase-only filters," Appl. Opt. **38**, 5004–5013 (1999).
24. V. Arrizón, U. Ruiz, R. Carrada, and L. A. González, "Pixelated phase computer holograms for the accurate encoding of scalar complex fields," J. Opt. Soc. Am. A **24**, 3500–3507 (2007).
25. T. Ando, Y. Ohtake, N. Matsumoto, T. Inoue, and N. Fukuchi, "Mode purities of Laguerre–Gaussian beams generated via complex-amplitude modulation using phase-only spatial light modulators," Opt. Lett. **34**, 34–36 (2009).
26. I. Moreno, A. Lizana, A. Márquez, C. Iemmi, E. Fernández, J. Campos, and M. J. Yzuel, "Time fluctuations of the phase modulation in a liquid crystal on silicon display: characterization and effects in diffractive optics," Opt. Express **16**, 16711–16722 (2008).
27. Y. Roichman, A. Waldron, E. Gardel, and D. G. Grier, "Optical traps with geometric aberrations," Appl. Opt. **45**, 3425–3429 (2006).
28. C. López-Quesada, J. Andilla, and E. Martín-Badosa, "Correction of aberration in holographic optical tweezers using a Shack-Hartmann sensor," Appl. Opt. **48**, 1084–1090 (2009).
29. Y. Roichman, I. Cholis, and D. G. Grier, "Volumetric imaging of holographic optical traps," Opt. Express **14**, 10907–10912 (2006).

1. Introduction

Optical microparticle manipulation by a single-beam trap is a well-known tool with numerous applications in the fields of biology, chemistry and physics [1]. It is usually studied at the focal plane of a microscope's objective where a particle may be trapped or moved along certain trajectory according to the field distribution of the applied beam. Different types of beams have been proposed for this task. For example, optical vortices such as the helical Laguerre-Gaussian (LG) modes yield rotation of a dielectric particle around the beam axis [2–4]. The rotation velocity depends on the orbital angular momentum carried by the beam, apart from the particle's characteristics (weight, size, form, material, etc.) and the surrounding medium. Certain combinations of the LG modes produce spiral beams [5–7] which maintain the form of their transversal intensity distribution apart from rotation and scaling. Such a type of beam was used for example in order to induce the Archimedes spiral movement of the particle [8]. On the other side, the sum of LG modes with opposite topological charge was found useful for particle sorting [9, 10].

Apart from setups designed for plane-curve particle movements, there are more sophisticated trapping systems based on a spatial light modulator (SLM) which provide an interactive three dimensional (3D) control of the particle position almost in real time [11, 12]. These systems, commonly known as optical tweezers, use the computer generated holograms (CGHs) that allow the fast optical beam modification for particle manipulation. They play a relevant role in many applications ranging from the measurement of biological forces to the construction

#139978 - $15.00 USD Received 21 Dec 2010; revised 10 Feb 2011; accepted 13 Feb 2011; published 4 Mar 2011

of micro-machines and micro-components [12], but a high amount of computational resources is required for real time synthesis of the CGHs. Nevertheless pre-designed 3D particle movements which are important for example for micro-robotics, can be induced by a single-beam trap. Notice that such an optical setup might use an analogue hologram for beam generation and therefore it is more compact and cheap than using a single SLM [5].

In this work, we study micro-particle's 3D movements induced by a single-beam trap given as a collinear superposition of the LG modes. The LG modes present a well-defined conical structure in the minimum beam-waist region. Correspondingly, the strongly focused beams over the sample constructed from the LG modes allow to form optical funnels or pods of different configurations depending on the mode indices, weights, waist, etc. In next section we describe the beams chosen for this study. A conventional holographic optical tweezers setup, considered in section 3, is used for the observation of particle-light interaction. Since the quality of the beam and the visualization of particle movement are essential for the correct interpretation of the results we also shortly discuss the methods used for CGH encoding and particle tracking. The movements of dielectric particles suspended in water induced by the optical beams are analyzed in section 4. The paper ends with concluding remarks and perspectives for future research.

2. Beam design for the optical trap

As basic elements for the optical beam-trap design we use linearly polarized monochromatic helical LG modes given by [13]

$$\mathrm{LG}_{p,l}^{\pm}(\mathbf{r};z) = w^{-1}(z)\sqrt{\frac{2\,p!}{\pi\,(p+l)!}}\left(\sqrt{2}\frac{x\pm iy}{w(z)}\right)^{l}\mathscr{L}_{p}^{l}\left(\frac{2r^{2}}{w^{2}(z)}\right) \times \exp\left(-\frac{r^{2}}{w^{2}(z)}\right)\exp\left(-i\frac{\pi r^{2}}{\lambda R(z)}\right)\exp\left(-i\,(2p+l+1)\,\zeta(z)\right), \tag{1}$$

with $\mathbf{r}=(x,y)$ being a transversal position vector, $r^2=x^2+y^2$, $w(z)=w_0\left(1+(z/z_R)^2\right)^{1/2}$, where w_0 is the minimum beam waist at the propagation distance $z=0$, $z_R=\pi w_0^2/\lambda$ being Rayleigh range, $\zeta(z)=\arctan(z/z_R)$ corresponding to Gouy phase, and $R(z)=z(1+(z_R/z))^2$ representing the wavefront curvature radius. Here $\mathscr{L}_p^l$ stands for the Laguerre polynomial with radial index p and azimuthal index l. This choice is explained by mode orthonormality, stability under the propagation through the isotropic paraxial systems (which besides a well-known limitations remain a good model for the conventional optical tweezers) and simple expression for the longitudinal component of the orbital angular momentum (OAM), J_z, carried by one mode or their linear superposition [14].

It has been reported in numerous publications that the beams carrying OAM produce particle rotation at the trapping plane, see for example [2–4]. Nevertheless, to the best of our knowledge, the obvious 3D spiral like trajectory of the particle in the neighbourhood of the focal plane has not been observed yet. Thus, one of the beam trap used for this study is a single helical LG mode

$$\mathscr{T}_1(\mathbf{r}) = \mathrm{LG}_{1,18}^{+}(\mathbf{r};0), \tag{2}$$

carried the global OAM $J_z=18$. The choice of the beam indices as well as its waist parameter is explained by the limitations of our experimental setup (named, laser power, numerical aperture of the objective, particle size, etc.) and is not relevant for further discussions.

We underline that two beams may have the same OAM but their interaction with a particle may differ due to the different intensity and OAM density distributions, which play an important role in the optical trap performance. The OAM density distribution of a beam constructed as a

#139978 - $15.00 USD Received 21 Dec 2010; revised 10 Feb 2011; accepted 13 Feb 2011; published 4 Mar 2011

linear superpositions of the LG modes $\sum_{p,l} a_{p,l} \mathrm{LG}^{\pm}_{p,l}(\mathbf{r};0)$, where $a_{p,l}$ are constants, is given by the expression [15]

$$j_z(\mathbf{r}) = \sum_{p,l,p',l'} \pm \left|a_{p,l}\right|^2 \left|\mathrm{LG}^{\pm}_{p,l}(\mathbf{r};0)\right|^2 l \pm \mathrm{Re}\left[a^*_{p,l} a_{p',l'} \mathrm{LG}^{\mp}_{p,l}(\mathbf{r};0)\,\mathrm{LG}^{\pm}_{p',l'}(\mathbf{r};0)\right](l'+l). \quad (3)$$

It is easy to see that the OAM density for a single LG mode is proportional to the intensity distribution $j_z(\mathbf{r}) = \pm\left|\mathrm{LG}^{\pm}_{p,l}(\mathbf{r};0)\right|^2 l$. The global OAM, J_z, is obtained by integration over the x and y coordinates: $J_z = \sum_{p,l} \pm \left|a_{p,l}\right|^2 l$.

To study the dependence of particle trajectory from the OAM density distribution we use the following superposition of the LG modes

$$\mathscr{F}_2(\mathbf{r}) = \left[\mathrm{LG}^{+}_{1,17}(\mathbf{r};0) + \mathrm{LG}^{+}_{1,19}(\mathbf{r};0)\right]/\sqrt{2}, \quad (4)$$

with the same global OAM, $J_z = 18$, and similar beam size as $\mathscr{F}_1$. Moreover $\mathscr{F}_2$ belongs to the class of the spiral beams mentioned above. From the analysis of mode indices it can be concluded (see for example [6, 7]) that the intensity distribution of $\mathscr{F}_2$ performs clockwise rotation at $\pi/2$ during free space propagation. The beam focusing accelerates the rotation near the focal plane. Notice that opposite rotation corresponds to the complex conjugate beam $\mathscr{F}_2^*$.

The next beam of interest is a linear combination of the LG modes with the same intensity distributions and opposite sign of OAM values,

$$\mathscr{F}_3(\mathbf{r}) = \left[\mathrm{LG}^{+}_{1,18}(\mathbf{r};0) + \mathrm{LG}^{-}_{1,18}(\mathbf{r};0)\right]/\sqrt{2}. \quad (5)$$

It is clear that this beam has zero OAM, and therefore it is expected that the trapped particle will not follow a spiral-like trajectory as in the previous case of the two other beams.

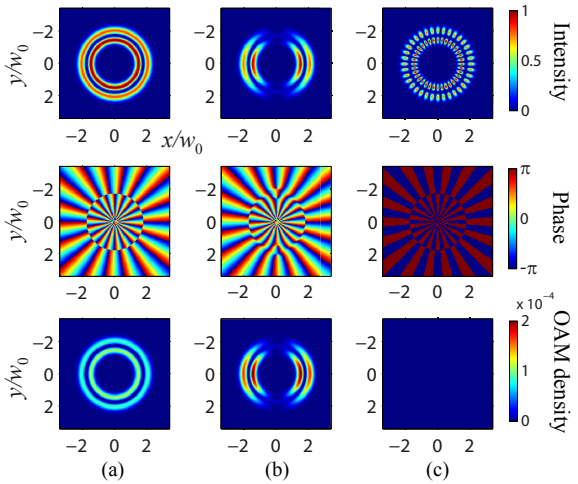

Fig. 1. Intensity, phase and OAM density distributions of the beams $\mathscr{F}_1$ (a), $\mathscr{F}_2$ (b), $\mathscr{F}_3$ (c), displayed in the first, second and third row respectively, at the minimum beam waist plane $z = 0$.

The intensity, phase and OAM density distributions of these three beams are shown in Fig. 1. We observe that the maxima of the OAM densities almost coincide with the maxima of the

#139978 - $15.00 USD Received 21 Dec 2010; revised 10 Feb 2011; accepted 13 Feb 2011; published 4 Mar 2011

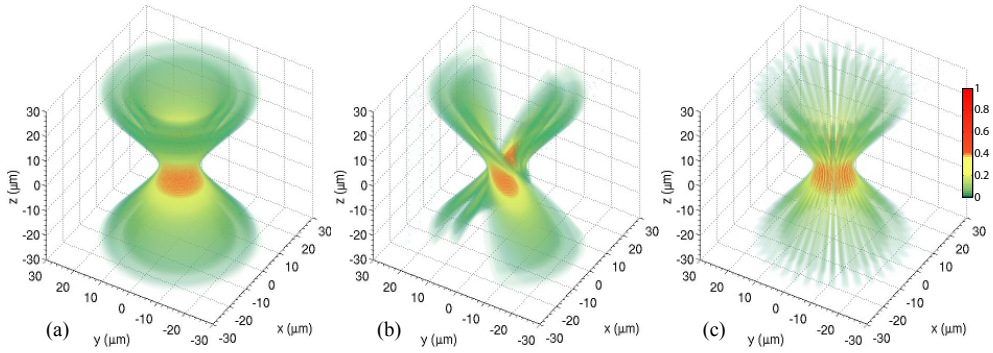

Fig. 2. Three-dimensional representation for the propagation of beams $\mathscr{F}_1$ (a), $\mathscr{F}_2$ (b), $\mathscr{F}_3$ (c). Minimum beam waist $w_0 = 3\,\mu$m is obtained at focal plane ($z = 0$) of the 100× microscope's objective lens.

intensity distribution for $\mathscr{F}_1$ and $\mathscr{F}_2$. The nonuniform distribution of the OAM over the rings for $\mathscr{F}_2$ yields to the larger OAM density in some regions and smaller for others than for $\mathscr{F}_1$. It is expected that particle plane rotation induced by $\mathscr{F}_2$ will be limited by the region with large OAM density and intensity distribution.

All three beams form a funnel-like structure in the neighbourhood of the focal plane ($z = 0$) as it can be appreciated from Fig. 2. For the numerical simulations we used the parameters corresponding to the experimental setup: a 100× microscope objective lens (MO) with 1.32 NA, wavelength $\lambda = 532$ nm and 0.25× relay optics (telescope). Then a minimum beam waist value of $w_0 = 3\,\mu$m is reached at the focal plane of the MO. As observed in Fig. 2, while the $\mathscr{F}_1$ and $\mathscr{F}_3$ beams remain invariant (except scaling), the $\mathscr{F}_2$ one presents an additional clockwise rotation yielding a double helix intensity structure. We also note, that since the diameter of the particle used in the experiments for the analysis of 3D movement is $10\,\mu$m, then the average intensity distribution over the particle cross-section is almost the same for the beams $\mathscr{F}_1$ and $\mathscr{F}_3$. Therefore the main difference in their interaction with the particle is the presence of the OAM in the case of $\mathscr{F}_1$ beam.

It is also possible to design other attractive trapping beams by combining two or more optical funnels. Along the last decade, different techniques were proposed to generate beams with cylindrical hollow axial structure (so-called optical bottles) [16–18]. Here we consider the collinear superposition of two optical funnels with a controlled focusing for each one then allowing generation a beam with pod-like structure. Indeed the position of the minimum beam waist value can be displaced a distance d away from the focal plane by modulating the input beam $\mathscr{F}_n(\mathrm{r})$ with a spherical phase distribution

$$g(d) = \exp\left(i2\pi n_{md}\frac{r^2}{\lambda \mathrm{f}^2}d\right), \tag{6}$$

where f is the focal length of the microscope objective lens and n_{md} is the refractive index of the medium (water in our case). Then several optical funnels focused at different distances can be combined to construct a tubular-like trap. In this work we consider the superposition of two optical funnels described as

$$\mathscr{P}_{n,m}(\mathbf{r}) = a_1\mathscr{F}_n^*(\mathbf{r}) + a_2\mathscr{F}_m(\mathbf{r}), \tag{7}$$

where $a_{1,2} = |a_{1,2}|\,g(d_{1,2})$ is the weight complex function that takes into account the focusing shift. In particular, we study the $\mathscr{P}_{1,1}$ and $\mathscr{P}_{2,2}$ beams with $a_1 = g(d)/\sqrt{2}$, $a_2 = 1/\sqrt{2}$ and

#139978 - $15.00 USD Received 21 Dec 2010; revised 10 Feb 2011; accepted 13 Feb 2011; published 4 Mar 2011

$d = -20\,\mu$m that yields a tubular pod-like structure near to the focal region as displayed in Fig. 3(a) and 3(b), respectively. The peculiarity of these beams lies in the change of the OAM sign of their part interacting with the particle. Thus, it is expected to observe the particle rotation at the opposite directions at different distances z.

The cross sections of the intensity distribution for all beams studied in this work at the distances $z = 0$ (first row) and $z = -11\,\mu$m (second row) are shown in Fig. 4.

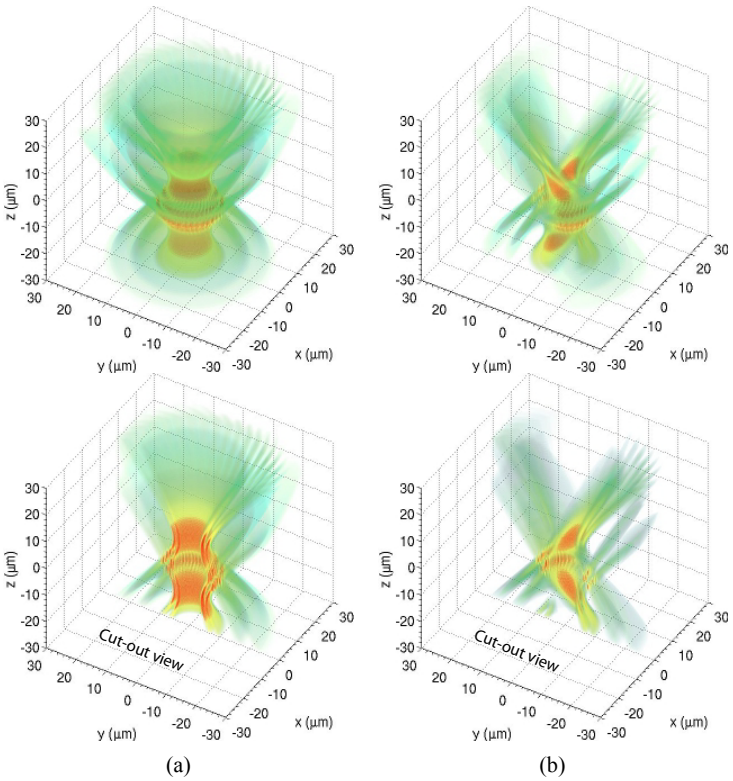

Fig. 3. Three-dimensional representation for the propagation of beam $\mathscr{P}_{1,1}$ (a) and $\mathscr{P}_{2,2}$ (b). To help visualization a 3D cut-out view of such beams is displayed in the second row.

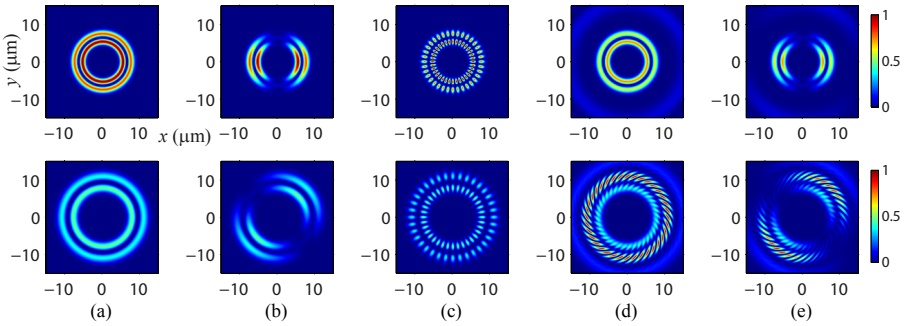

Fig. 4. Transversal intensity distributions for propagation distance $z = 0$ (first row) and $z = -11\,\mu$m (second row) for the beams: $\mathscr{F}_1$ (a), $\mathscr{F}_2$ (b), $\mathscr{F}_3$ (c), $\mathscr{P}_{1,1}$ (d) and $\mathscr{P}_{2,2}$ (e).

#139978 - $15.00 USD Received 21 Dec 2010; revised 10 Feb 2011; accepted 13 Feb 2011; published 4 Mar 2011

3. Experimental implementation

To generate these trapping beams we used a conventional holographic optical tweezers setup (see Fig. 5), which consists from a hand-made inverted light microscope with Zeiss 100× objective (1.32 NA, oil immersion, Plan-Apochromat), a reflective LCoS-SLM (Holoeye LCR-2500, twisted nematic, 8-bit grayscale signal, pixel size $\delta = 19\ \mu$m) operating in phase-only modulation, and Nd:YAG laser with wavelength $\lambda = 532$ nm and 400 mW. Theory and experimental implementation of such systems are studied in [19] and [20], to name a few. The CGH is addressed onto a phase-only SLM that modulates a collimated laser beam. The resulting beam, B1, is focused over the sample by using a Keplerian telescope and the microscope objective, as sketched in Fig. 5.

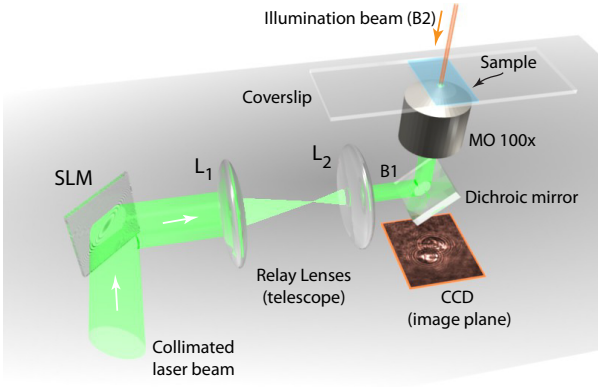

Fig. 5. Schematic representation of the holographic optical trapping system. SLM displays the hologram that is imaged into the back focal plane of the microscope objective (MO) by using two relay lenses, L_1 and L_2, working as 0.25× telescope. The sample is illuminated by an additional laser beam B2 in order to acquire its image as in-line hologram, which is recorded in real time by a CCD camera.

Particle tracking is achieved by using an additional collimated laser beam B2 (in our case $\lambda = 532$ nm and 10 mW) that replaces the conventional incandescent illuminator, see Fig. 5. Its irradiance is comparable to that of conventional microscope illumination and therefore it does not exert measurable forces on the illuminated particles (suspended in the sample). Light scattered by the sample is recorded by a CCD camera (pixel size of $4.6\,\mu$m and 30 frames per second) in real time as an in-line hologram, which can be numerically analyzed in order to obtain the 3D particle position. In this work we use Rayleigh-Sommerfeld (RS) back-propagation for the in-line hologram reconstruction because it permits faster particle tracking. This technique was studied in detail for holographic video microscopy in [21] and was found successful for micro-sized colloidal spheres of polystyrene and silica tracking. The in-line hologram results from interference between the light scattered by the particle and the unscattered portion of the illumination laser beam B2 at the focal plane of the objective. In our case this hologram is 100× magnified by the MO lens and recorded as a raw-video file by using a CCD camera (exposure time was 1 ms). The hologram reconstruction is achieved by computing the RS diffraction integral which makes possible to render a volumetric reconstruction of the light scattered by the particle. The particle's position is found by locating maxima in such a volumetric reconstruction [21].

Since the SLM operates in phase-only modulation, the beam complex amplitude distribution has to be encoded into the phase hologram. In the last decades several types of CGHs have been proposed to overcome this problem, see for example [22–24]. To shape both amplitude

#139978 - $15.00 USD Received 21 Dec 2010; revised 10 Feb 2011; accepted 13 Feb 2011; published 4 Mar 2011

and phase of the trapping beam we consider the method described in [24], that yields an accurate beam synthesis [25] ensuring its stability under propagation.

Let us now describe the beam generation approach. It is well-known [22] that an arbitrary scalar complex field described by $s(x,y) = a(x,y)\exp[i\phi(x,y)]$, where $a(x,y)$ and $\phi(x,y)$ are the amplitude and phase distribution respectively, can be encoded as a phase CGH with a transmittance function $H(x,y) = \exp[i\psi(a,\phi)]$. To obtain an appropriate dependence of $\psi(a,\phi)$, function $H(x,y)$ has to be represented as a Fourier expansion in the domain of $\phi(x,y)$. As demonstrated in [24], the encoded signal $s(x,y)$ is recovered from first-order term of such Fourier expansion by using the following hologram phase modulation:

$$\psi(a,\phi) = f(a)\sin\phi, \tag{8}$$

provided that the condition $J_1[f(a)] = a$ is fulfilled for every value of amplitude $a(x,y)$ in the interval $[0,1]$, by choosing the appropriate value of $f(a)$ according to Bessel function $J_1(\rho)$. To isolate the encoded field $s(x,y)$ from the other terms of the Fourier expansion it is necessary to perform spatial filtering by adding a linear carrier phase $\varphi_c = 2\pi(u_0 x + v_0 y)$, with spatial frequencies (u_0, v_0), to the phase of the encoded field. Fortunately, this spatial filtering can be optically achieved using the Keplerian telescope (4-f system), see Fig. 5, where the SLM is placed at the back focal plane of the first relay lens. Notice that the reconstruction of the encoded signal $s(x,y)$ is performed by spatial filtering of the first-order difracction term in the CGH Fourier spectrum plane [24]. In our case the overall diffraction efficiency (light guided into the first diffraction order) of the LCoS display is about 45%, see [26] for further details. Because of such a filtering process the maximum beam output power is about one half of the one corresponding to the input collimated beam.

Wavefront distortion φ_{ab} arising from the SLM non-flatness, mainly astigmatism and spherical aberration, was calibrated following the suggestions reported in [20]. The SLM also allows compensating the wavefront aberrations corresponding to the optical setup, see Refs. [27, 28]. To compensate such aberrations and therefore to optimize the optical trap performance, the hologram phase modulation Eq. (8) is evaluated as $\psi(a, \phi - \varphi_{ab} + \varphi_c) \bmod 2\pi$. Notice that aberrations such as coma and astigmatism mainly degrade the lateral trapping efficiency while the spherical aberration mostly degrades the axial trapping performance [27]. A further wavefront correction can be achieved as proposed in [28].

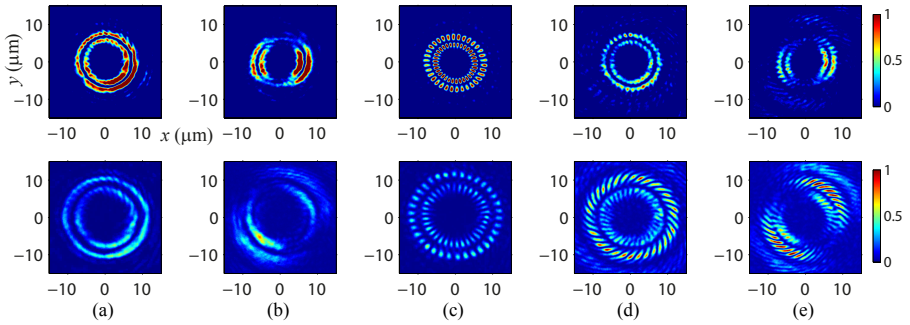

Fig. 6. Experimental results (Media 1): Transversal sections at $z = 0$ (first row) and $z = -11\,\mu$m (second row) for the beams: $\mathscr{F}_1$ (a), $\mathscr{F}_2$ (b), $\mathscr{F}_3$ (c), $\mathscr{P}_{1,1}$ (d) and $\mathscr{P}_{2,2}$ (e).

The corrected beam B1 is focused over the sample, which is enclosed into a flow cell made by attaching a glass coverslip (thickness 0.17 mm) to a standard microscope slide with double-sided tape, see Fig. 5. The coverslip partially reflects the trapping light back into the objective lens which images this beam through a 90% dichroic mirror (at wavelength $\lambda = 532$ nm) to

#139978 - $15.00 USD Received 21 Dec 2010; revised 10 Feb 2011; accepted 13 Feb 2011; published 4 Mar 2011

the CCD camera, see Fig. 5. Then it is possible to obtain a volumetric reconstruction of the trapping light by translating the coverslip with respect to the objective lens. This approach has been previously demonstrated in [29] by using a mirror instead of a coverslip. In this work we use the coverslip for this task because it allows in-situ testing of the beam degradation caused by its lack of flatness. Figure 6 shows the intensity distributions of the trapping beams corresponding to the optical funnel $\mathscr{F}_1$ (a), $\mathscr{F}_2$ (b) and $\mathscr{F}_3$ (c) and the optical pods $\mathscr{P}_{1,1}$ (d) and $\mathscr{P}_{2,2}$ (e), measured by translating the coverslip (see also Media 1). These experimental results are in good agreement with the numerical simulations displayed in Fig. 4. Nevertheless there exists a wavefront distortion due to the residual aberrations of the optical setup, which may be minimized by performing further wavefront correction as reported in [28]. In the next section we study the action of these beams over polystyrene spheres suspended in distilled water.

4. Microparticle manipulation: experimental results

We start from the analysis of particle movements ($2\,\mu$m diameter polystyrene sphere, Spherotech SPV-20-5 Lot W01) at the focal plane of the MO, which in this case is near to the upper covering glass in order to compensate the axial scattering force. Figure 7 shows the motion of the trapped particle along the multiringed beam profile following the exerted torques (see also Media 2 and Media 3). As expected, the particle is confined in the high-intensity circular fringes and rotates around the beam $\mathscr{F}_1$ axis whereas for the case of beam $\mathscr{F}_2$ it only rotates in the angular range limited by the nonzero OAM density. The trapping with the beam $\mathscr{F}_3$ does not produce any rotation due to zero OAM density.

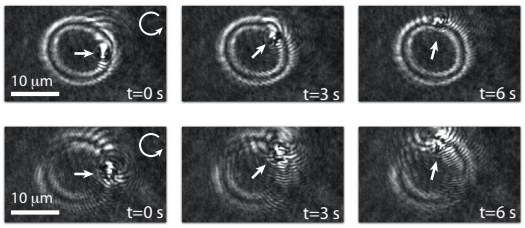

Fig. 7. In-line holograms showing the trapped particle ($2\,\mu$m diameter) for the beam $\mathscr{F}_1$ Media 2 and $\mathscr{F}_2$ Media 3, first and second row respectively.

Let us now consider the 3D motion of $10\,\mu$m diameter polystyrene spheres (Duke Scientific Lot 9949) suspended in water, which is induced by the proposed trapping beams. The flow-cell thickness is about $120\,\mu$m and the particle motion starts from the lower coverslip surface. Figure 8(a)–8(c) displays the particle's tracking for the beams $\mathscr{F}_1$, $\mathscr{F}_2$ and $\mathscr{F}_3$, respectively. Although both beams $\mathscr{F}_1$ and $\mathscr{F}_2$ have the same OAM ($J_z = 18$), they exert different forces and torques on the particle according to the geometry of their 3D intensity and OAM density distributions. This yields different types of helix-like trajectories, see Fig. 8(a) Media 4 and Fig. 8(b) Media 5. In contrast, the beam $\mathscr{F}_3$ does not transfer OAM and therefore the particle just goes up to the minimum beam waist plane ($z = 0$), see Fig. 8(c). Notice that these trapping beams are displayed for the trap-region of interest, given between the lower coverslip surface at $z = -30\,\mu$m and the focal plane $z = 0$. Several video snapshots corresponding to the in-line holograms obtained for the case $\mathscr{F}_1$, $\mathscr{F}_2$ and $\mathscr{F}_3$ are also showed in Fig. 8(d)–8(f). We underline that clockwise rotation direction is obtained for the complex conjugate beams $\mathscr{F}_1^*$ and $\mathscr{F}_2^*$.

Since the intensity distribution of the beams $\mathscr{F}_1$ and $\mathscr{F}_3$ posses angular symmetry the particle may be trapped in any point of the plane where the light force is sufficient, while for the beam $\mathscr{F}_2$ there are two well-defined regions around the intensity maxima where it may happens. Moreover, due to the relatively big particle size, two particles can be simultaneously trapped

#139978 - $15.00 USD Received 21 Dec 2010; revised 10 Feb 2011; accepted 13 Feb 2011; published 4 Mar 2011

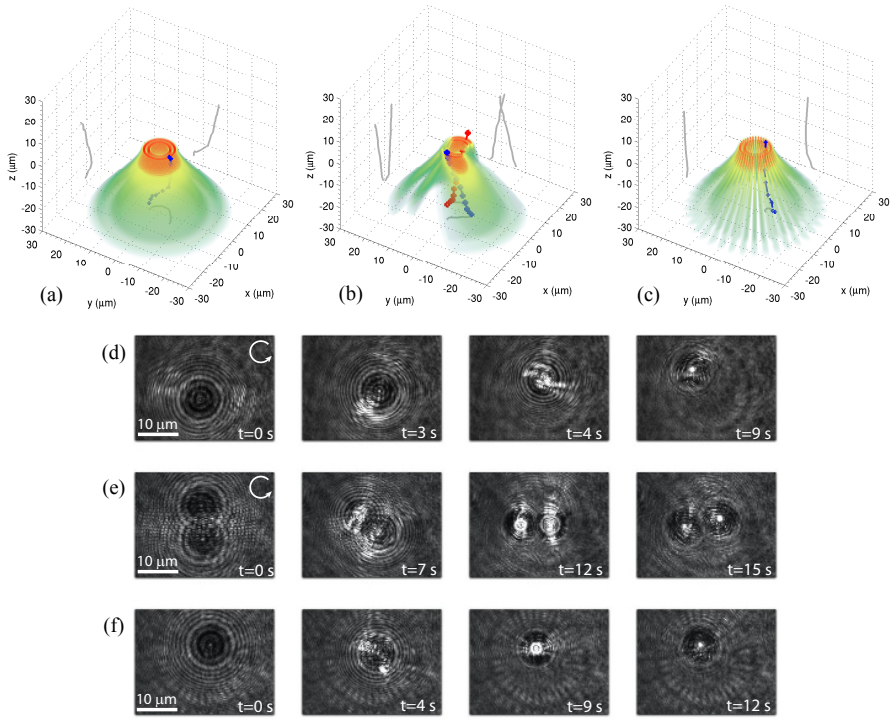

Fig. 8. 3D particle-tracking reconstruction for the beams: $\mathscr{F}_1$ (a) Media 4, $\mathscr{F}_2$ (b) Media 5, $\mathscr{F}_3$ (c). Particle's trajectory is also projected into $x-y$, $x-z$ and $y-z$ planes (grey lines). It is experimentally measured from in-line holograms stored as video as the ones showed in (d) Media 6, (e) Media 7, and (f), correspondingly. The trajectories start from the lower coverslip surface at $t=0$ s ($z=-30\,\mu$m) and ends at the focal plane $z=0\,\mu$m.

by beam $\mathscr{F}_2$ following different helical channels as it is observed in Fig. 8(b) and 8(e). This may be useful for the organization of different sorting particle flows in the same cell for the observation of their interaction in the focal plane.

While the direction of the particle rotation trapped by the considered optical funnels is fixed, it may varies with the distance for the pod-like structures. As an example, we consider the 3D particle movement induced by the beam $\mathscr{P}_{1,1}$. Figure 9(a) together with Media 8 show the particle trajectory. For better visualization a cut-out view of the beam and the particle's trajectory are represented in Fig. 9(b). The video snapshots, several of them are presented in Fig. 9(c), corresponding to the in-line holograms used for the 3D particle-tracking reconstruction are found in Media 9. In this case the particle describes a spiral trajectory from the starting point A [$z=-30\,\mu$m, see Fig. 9(b)] with clockwise rotation (due to the $\mathscr{F}_1^*$ beam), until it reaches the distance $z=-25\,\mu$m corresponding to the point B. At this point the particle is simultaneously trapped by both optical funnels $\mathscr{F}_1^*$ and $\mathscr{F}_1$, which exert opposite torques over the particle according with their OAM value ($J_z=\mp 18$, respectively). Therefore the particle goes straight up until the point C, in which its interaction with the $\mathscr{F}_1$ becomes stronger. From the point C to D the particle, as expected, follows a new spiral trajectory with anticlockwise rotation. The relatively short elevation (with respect to the funnel trapping) of the particle during spiral movement (A-B and C-D tracks) is explained by the fact that only one half of the beam energy is participated in light-particle interaction in these regions. We underline that the movements

#139978 - $15.00 USD Received 21 Dec 2010; revised 10 Feb 2011; accepted 13 Feb 2011; published 4 Mar 2011

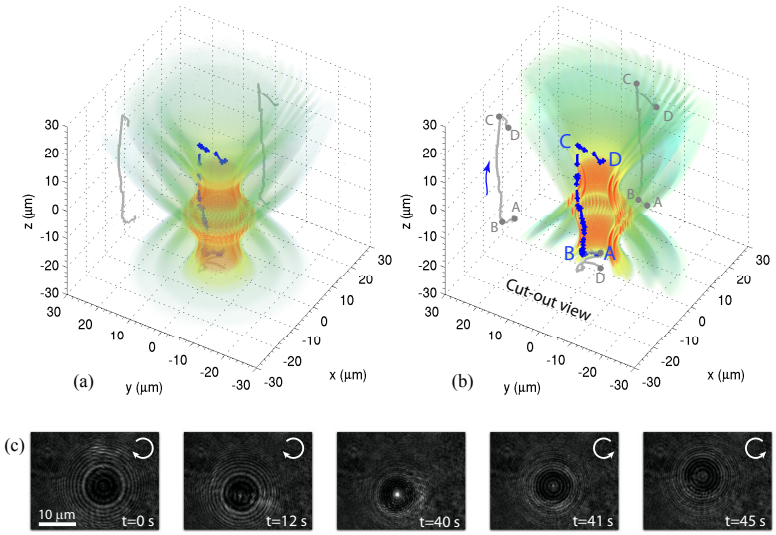

Fig. 9. 3D particle-tracking reconstruction for the trapping beam $\mathscr{P}_{1,1}$ (a) Media 8 and (b). Particle's trajectory is also projected into $x-y$, $x-z$ and $y-z$ planes (grey lines). The in-line holograms (as the ones shown in (c)) used for the reconstruction are stored as video, see Media 9 .

of such particles, induced by the designed beams, have been systematically reproduced. For smaller polystyrene sphere the longer spiral trajectories are expected due to the lager longitudinal regions where the particle is trapped by only one of the funnels ($\mathscr{F}_1^*$ or $\mathscr{F}_1$) composed the pod.

This pod beam allows trapping of multiple particles, which simultaneously rotate in clockwise and anticlockwise directions at different distances z. It could be useful for twisting of rod-like particles or filaments which ends are trapped in the regions with opposite OAM sign.

5. Conclusions

The design of funnel and pod beams suitable for volumetric optical trapping and the method for their correct generation have been discussed. The interaction of these beams with dielectric colloidal particles was experimentally observed. It has been demonstrated that the trapped particles describe a 3D spiral trajectory governed by the forces and torques exerted by the beam carrying OAM. In contrast to a single helical-LG funnel the double-helix funnel beam provides two well-defined 3D channels for the particle movement. The capacity of the proposed bifocal pod beam to exert opposite particle rotations, at different planes during its propagation, is attractive for various micro-object manipulation techniques including all-optical twisting. Moreover the trapping of a rod-like particle by a similar pod beam with the same OAM sign in both focal regions could be used for optically driven stirring or pumps. These facts result useful for volumetric trapping and provide an additional level of control over the trapped particles. The manipulation of particles with different geometries, size and material by these and other funnel and pod beams will be the subject of further research.

While the described setup uses the SLM for the single-beam trap generation, the application of analogue hologram for this task will significantly increase the energetic layout of such optical traps providing setup compactness and reducing its cost.

#139978 - $15.00 USD Received 21 Dec 2010; revised 10 Feb 2011; accepted 13 Feb 2011; published 4 Mar 2011

Acknowledgments

The financial support of the Spanish Ministry of Science and Innovation under projects TEC2008-04105, TEC2009-5545-E/TEC are acknowledged. J. A. Rodrigo and A. M. Caravaca-Aguirre gratefully thank a "Juan de la Cierva" grant and fellowship from "Obra Social Ibercaja (Beca Ibercaja de Investigación 2010)", respectively. The authors appreciate valuable comments from J. R. Arias-González.

#139978 - $15.00 USD Received 21 Dec 2010; revised 10 Feb 2011; accepted 13 Feb 2011; published 4 Mar 2011